



HAL
open science

High-Temperature Radiative Behavior of an $\text{La}_2\text{NiO}_{4+\delta}$ Cathodic Layer for SOFCs (up to 900°C): Influence of δ and Texture

Minh Tri Ta, Benoit Rousseau, Leire del Campo, Julien-Yves Rolland, Stéphanie Touchefeu, Emmanuel Veron, Domingos de Sousa Meneses, Patrick Echegut, Pascal Lenormand, Florence Ansart

► To cite this version:

Minh Tri Ta, Benoit Rousseau, Leire del Campo, Julien-Yves Rolland, Stéphanie Touchefeu, et al.. High-Temperature Radiative Behavior of an $\text{La}_2\text{NiO}_{4+\delta}$ Cathodic Layer for SOFCs (up to 900°C): Influence of δ and Texture. *Journal of the American Ceramic Society*, 2011, 94 (8), pp.2535-2541. 10.1111/j.1551-2916.2011.04446.x . hal-03472037

HAL Id: hal-03472037

<https://hal.science/hal-03472037>

Submitted on 9 Dec 2021

HAL is a multi-disciplinary open access archive for the deposit and dissemination of scientific research documents, whether they are published or not. The documents may come from teaching and research institutions in France or abroad, or from public or private research centers.

L'archive ouverte pluridisciplinaire **HAL**, est destinée au dépôt et à la diffusion de documents scientifiques de niveau recherche, publiés ou non, émanant des établissements d'enseignement et de recherche français ou étrangers, des laboratoires publics ou privés.



Open Archive Toulouse Archive Ouverte (OATAO)

OATAO is an open access repository that collects the work of Toulouse researchers and makes it freely available over the web where possible.

This is an author-deposited version published in: <http://oatao.univ-toulouse.fr/>
Eprints ID: 5714

To link to this article: DOI: 10.1111/j.1551-2916.2011.04446.x
URL : <http://dx.doi.org/10.1111/j.1551-2916.2011.04446.x>

To cite this version:

Ta, Minh Tri and Rousseau, Benoit and Del Campo, Leire and Rolland, Julien-Yves and Touchefeu, Stéphanie and Veron, Emmanuel and De Sousa Meneses, Domingos and Echehut, Patrick and Lenormand, Pascal and Ansart, Florence *High-Temperature Radiative Behavior of an $\text{La}_2\text{NiO}_{4+\delta}$ Cathodic Layer for SOFCs (up to 900°C): Influence of δ and Texture*. (2011) Journal of the American Ceramic Society, vol. 94 (n° 8). pp. 2535-2541. ISSN 0002-7820

Any correspondence concerning this service should be sent to the repository administrator: staff-oatao@listes.diff.inp-toulouse.fr

High-Temperature Radiative Behavior of an $\text{La}_2\text{NiO}_{4+\delta}$ Cathodic Layer for SOFCs (up to 900°C): Influence of δ and Texture

Minh Tri Ta,^{*,‡} Benoit Rousseau,^{†,‡} Leire del Campo,[‡] Julien-Yves Rolland,[‡] Stéphanie Touchefeu,[‡]
Emmanuel Veron,[‡] Domingos De Sousa Meneses,[‡] Patrick Echegut,[‡] Pascal Lenormand,[§]
and Florence Ansart[§]

[‡]CEMHTI CNRS, UPR 3079 Orléans Cedex 2, France

[§]CIRIMAT-LCMIE, UMR CNRS 5085, 31062 Toulouse Cedex 9, France

Thermal radiation is likely to play an important role in the calculation of the energy balance in solid oxide fuel cells (SOFCs), due to their high operating temperatures ($600^\circ\text{--}1000^\circ\text{C}$). However, the majority of previous studies dealing with this issue have used room-temperature radiative data for determining the overall heat transfer process within a given cell, which could lead to an inexact appreciation of the role played by the thermal radiation. Consequently, the thermal field within the cell could also be incorrectly determined; however, accurate knowledge of the thermal field is important in order to understand the mechanical behavior of SOFCs. Several parameters, including chemical composition, texture, thickness, and of course operating temperature, have a large effect on the radiative properties of a given compound. As a first step to elucidate the temperature-dependent behavior of SOFCs, we deposited an $\text{La}_2\text{NiO}_{4+\delta}$ cathodic layer on a planar $\text{ZrO}_2\text{--}8\%\text{ Y}_2\text{O}_3$ electrolyte-supported SOFC and investigated its radiative properties using high-temperature infrared emissivity spectroscopy ($100^\circ\text{--}900^\circ\text{C}$). Additional X-ray diffraction, thermo-gravimetric analysis, and environmental scanning electron microscopy measurements were also made to study the role played by both the chemical composition and texture on the radiative properties of the cell.

I. Introduction

THE solid oxide fuel cell (SOFC) is a promising technology for future power generation because it offers a clean, quiet, and highly efficient energy solution by comparison with conventional systems. Depending on the materials used, SOFCs usually operate at high temperatures (typically $600^\circ\text{--}1000^\circ\text{C}$). Unfortunately, these operating conditions can lead to mechanical stresses within the cell (cathode/electrolyte/anode) caused by large thermal gradients^{1,2} existing both internally or at the contact points with metallic interconnectors.

In order to understand the thermal behavior of SOFCs and to improve the thermo-mechanical properties, knowledge of their temperature fields is particularly important.³ In this respect, for a plane geometry, it appears a relatively straightforward procedure to incorporate the radiative contributions into numerical codes dealing with mass and heat transfer.^{4–6} However, precise results are precluded by the lack of thermo-physical data, i.e., thermal conductivity and radiative properties of the materials used in SOFCs at operating temperatures. Moreover, the materials used in SOFCs are often textured ceramics, which leads to

an even more difficult prediction of the thermal radiative properties (TRPs) (reflectivity, transmittivity, and emissivity). Although optics-based studies have been performed previously on SOFC materials, including Raman^{1,2} and *in situ* potential-dependent Fourier transform infrared (FTIR) emission spectroscopy,⁷ the experimental measurement of TRPs requires extensive further investigation, especially at high temperature. In fact, very limited data are available even at room temperature.^{8,5,6} The term texture refers to the three-dimensional (3D) spatial distribution of grains and pores within the ceramic and their characteristic shape and size distribution. Furthermore, the texture of a ceramic also determines its porosity and its surface roughness. For a given material, the TRPs are influenced by its intrinsic and extrinsic features, which are themselves related to the chemical composition and texture. Recent investigations of material's multilength-scale characteristics show that it is possible to predict the TRPs from knowledge of the material's 3D structure and chemical composition.^{9–11} With the goal of performing such a numerical work on SOFC materials, it is necessary to first by measure their high-temperature radiative properties and second to characterize both their chemical composition and texture. These two steps are performed in this study.

In this work, a porous coating of $\text{La}_2\text{NiO}_{4+\delta}$,^{12,13} which is widely used as an SOFC cathode layer and operates at an intermediate temperature ($\sim 700^\circ\text{C}$),^{14–16} is studied. $\text{La}_2\text{NiO}_{4+\delta}$ is well known for having good electronic conductivity,¹⁷ which enhances its electrocatalytic activity in comparison with classical cathodic materials. Indeed, the good electronic conductivity leads to an increase in the number of available sites for reducing oxygen over the entire cathode volume, instead of limiting the reaction only to the triple phase boundary (TPB),¹⁸ and decreases the over-potential of the oxygen reduction reaction at the TPB.¹⁹ $\text{La}_2\text{NiO}_{4+\delta}$ is a mixed ionic–electronic conductor (MIEC) with a K_2NiF_4 -type structure,¹⁹ which can show a wide range of oxygen excess (δ).^{20–22} The insertion of oxygen relaxes the structural constraints of the undoped compound at the lattice scale. Then, it creates holes ($\text{Ni}^{2+} \rightarrow \text{Ni}^{3+}$) within the *ab* plane that can be trapped by the host lattice, i.e., polarons. The insertion of oxygen is responsible for the highly anisotropic properties^{23–25} of this compound. The polaronic carriers also lead to a broad absorption band in the mid-infrared range if they are trapped or a band localized in the far infrared range, with a diminishing tail, if they are mobile.^{26,27} The insertion of oxygen also controls the structural and physical (magnetic, electrical, and optical) properties.^{22,28} Previous studies report that, at room temperature, this oxide can behave as a semitransparent compound when δ is zero and, when δ increases to 0.25, it turns into an opaque compound for very low thicknesses (a few microns).²⁹ On the other hand, knowing the value of δ at high temperatures is crucial for predicting $\text{La}_2\text{NiO}_{4+\delta}$'s intrinsic TRPs. A previous study dealt with the influence of δ on the intrinsic TRPs of a $\text{Pr}_2\text{NiO}_{4+\delta}$ isostructural single crystal.³⁰

J. Stevenson—contributing editor

*Member, The American Ceramic Society.

[†]Author to whom correspondence should be addressed. e-mail: benoit.rousseau@univ-nantes.fr

In the following, we first describe the experimental methods used for characterizing the radiative, chemical, and textural properties of the porous $\text{La}_2\text{NiO}_{4+\delta}$ layer. We then present the radiative data (normal spectral emissivity). Finally, the radiative behavior of the layer is discussed with the purpose of providing a basis for future numerical predictive studies of TRPs or heat and mass transfer modeling.

II. Experimental Procedure

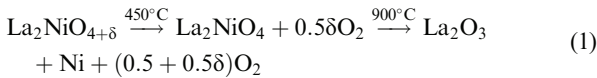
(1) Preparation of $\text{La}_2\text{NiO}_{4+\delta}$ Porous Layer

In this work, we use SOFC half-cells consisting of an electrolyte based on ZrO_2 -8% Y_2O_3 (YSZ) and an $\text{La}_2\text{NiO}_{4+\delta}$ functional layer. This layer was prepared by a sol-gel-modified process at CIRIMAT—Toulouse, France. More details on the preparation process can be found in Castillo and colleagues^{31,32}. A disk of polycrystalline YSZ was polished until its surface roughness (R_a) was < 10 nm. The surface was then cleaned by immersion in deionized water and dried in air before deposition. The layer was grown by dip-coating the YSZ in an $\text{La}_2\text{NiO}_{4+\delta}$ slurry. The average grain size of the $\text{La}_2\text{NiO}_{4+\delta}$ powder is around 200 nm. The layer was annealed in air at 1150°C with a temperature ramp of 2°C/min. Multistep deposition and annealing were necessary to achieve the desired increased thickness of the layers.¹²

(2) Layer Characterization

(A) *X-Ray Diffraction (XRD)*: The crystallographic structure of the layer was measured at 300 K using a Bruker D8 advance diffractometer ($\lambda_{\text{CuK}\alpha} = 0.15418$ nm). The acquisition time was 5 s with a step of 0.016°. The TOPAS software (Bruker, Karlsruhe, Germany) was used to determine the lattice parameters.

(B) *Thermo-Gravimetric Analysis (TGA)*: The intrinsic TRPs of $\text{La}_2\text{NiO}_{4+\delta}$ depend mainly on δ . Thus, it is crucial to determine the value of δ for the layer over the whole temperature range from 20° to 900°C. In practice, it is very difficult to perform TGA measurements directly on a thick (on the order of several micrometers) layer because the mass (< 1 mg for a 10 mm diameter and 5 μm thick pellet) is insufficient to obtain reliable results. Therefore, to determine δ , one can instead use the TGA method on the $\text{La}_2\text{NiO}_{4+\delta}$ starting powder used in the synthesis of the layer. Thus, 100 mg of powder was subjected to the same thermal cycle as experienced during the sintering of the deposited layer. The room-temperature value of δ of the starting powder was then obtained through a cycle of heating under a reducing atmosphere (95% Ar+5% H_2 flow with a temperature rate of 0.5°C/min) to completely decompose $\text{La}_2\text{NiO}_{4+\delta}$ into NiO and La_2O_3 according to the following decomposition scheme



For all the experiments, a thermo-balance (Setaram SETSYS Evolution 2400, sensitivity ± 1 μg , Caluire, France) was used to check the weight variation.

(C) *Environmental Scanning Electron Microscopy (ESEM)*: ESEM imaging measurements were performed at 27°C using a Philips FEI XL40 (Hillsboro, OR). The environmental method was used to study the $\text{La}_2\text{NiO}_{4+\delta}$ sample because it avoids the use of a metallization procedure that would otherwise interfere with subsequent optical studies. Moreover, the ESEM apparatus is equipped with a table that enables the acquisition of tilted ESEM images (with a small angle of tilting (0,+6°)). The Mex[®] (ALICONA, Graz, Austria) software was used to combine the tilted images to make a 3D image according to a stereoscopic method.

(D) *High-Temperature Infrared Emissivity Spectroscopy*: High-temperature (up to 900°C by CO_2 laser heating) infrared emissivity measurements were performed using an FTIR spectrometer (Bruker Vertex 80v) with a direct method.³³⁻³⁵ This method involves the comparison of the flux emitted by the heated sample with that emitted from a blackbody reference (Pyrox, PY8, Rambouillet, France). The sample holder and the blackbody are positioned on an automated rotation table (AEROTECH|ALAR-150, Pittsburgh, PA), which rearranges the sources at the focal point of the spectrometer. The heating of the sample is carried out with a CO_2 laser with a maximum power of 500 W. During an experiment, the laser beam is divided by a beam splitter into two equal parts allowing sample heating on both sides (see Fig. 1(a)). This optical configuration is useful for minimizing the axial temperature gradients within the sample area. Furthermore, because the laser beam has a Gaussian profile, only the sample's area ($\varnothing = 3$ mm) that is heated by the top of the beam is considered for the emissivity measurement. From this central area, where the temperature is homogenous, a smallest zone is selected with a diaphragm located on the optical path corresponding to the emitted flux in order to select an isothermal area of 1 mm-diameter on the sample (Figs. 1(b) and (c)). Thus, radial temperature gradients are also avoided. By combining both these precautions, the temperature homogeneity of the sample for emissivity measurement is guaranteed (the temperature difference in this zone is $\pm 5^\circ\text{C}$, thus the calculated error is $\pm 1\%$). A similar optical condition is applied for measuring the flux emitted by the blackbody. The whole system is placed in a chamber operating under a dry air purge to avoid absorption bands of H_2O and of CO_2 (see Fig. 1). According to De Sousa Meneses *et al.*,³⁴ the emittance of the sample can be determined by the knowledge of three interferograms acquired with identical temperatures for the blackbody reference and the sample, thus

$$E_s = \frac{\text{FT}(I_s - I_a)}{\text{FT}(I_{bb} - I_a)} \frac{L(\sigma, T_{bb}) - L(\sigma, T_a)}{L(\sigma, T_s) - L(\sigma, T_a)} \quad (2)$$

where FT designates the Fourier transform. I_a is the interferogram without sample measured under ambient conditions; I_{bb} is measured from a blackbody reference at temperature T_{bb} ; I_s is obtained with the sample positioned precisely at the focus point at temperature T_s . L_a , L_{bb} , and L_s are the radiative emissions predicted by Planck's law at temperatures T_a , T_{bb} , and T_s , respectively.

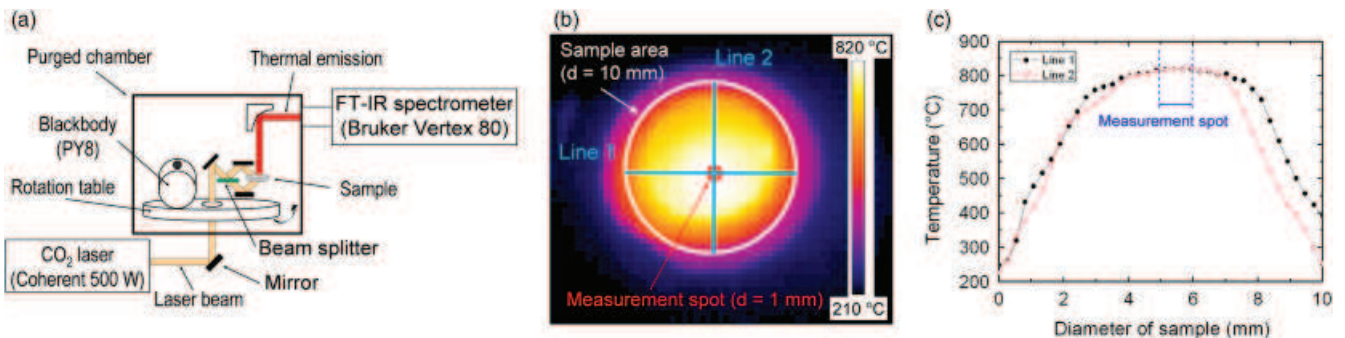


Fig. 1. Schematic diagram of the setup used for emissivity measurements (a), infrared imaging of sample under temperature (Flir ThermoCAM[®] SC 3000, Wilsonville, OR) (b), and selected area for minimizing temperature gradients in the sample (c).

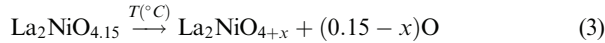
III. Results and Discussions

(1) Value of Excess Oxygen (δ) for the $\text{La}_2\text{NiO}_{4+\delta}$ Layer

Figure 2 shows the XRD pattern of the $\text{La}_2\text{NiO}_{4+\delta}$ layer deposited on a YSZ electrolyte substrate (thickness = 1 mm, diameter = 10 mm, porosity $\sim 3\%$). The diffraction peaks found at 30.1° , 34.9° , 50.2° , 59.6° , and 62.5° correspond to the polycrystalline YSZ substrate. The lattice parameters ($a = 5.36339$ Å, $b = 5.45679$ Å and $c = 12.688746$ Å) were refined using an orthorhombic ($Fmmm$) space group. However, the simple indexing of diffraction patterns cannot be used to determine the value of δ because X-rays are not very sensitive to light atoms such as oxygen. The neutron scattering length, on the other hand, is independent of atomic number and hence neutron diffraction is more sensitive to lightweight atoms including oxygen.³⁶ However, this technique requires a large sample volume, which is not available in this study because the total mass of the layer is relatively small.

To accurately measure the value of δ , we apply the method proposed by Rice and Buttrey²² and Hücker *et al.*³⁷ to the acquired diffractogram. In this method, the value of δ is extracted from the lattice parameters (a , b , c), which are obtained by observing the position of the $\text{La}_2\text{NiO}_{4+\delta}$ peaks. Oxygen incorporated into the La_2NiO_4 lattice leads to an increase of the “ c ” parameter. With the previously proposed chart,^{22,37} we can quantify the value of oxygen excess from the relationship between the ratio $\frac{2c}{a+b}$ and δ at $T = 300$ K. Thus, a value of $\delta = 0.14$ is found for the layer characterized by XRD at room temperature. A similar value (~ 0.15) was obtained for the starting powder by TGA under a reducing atmosphere (see Fig. 3).

Figures 4(a) and (b) show the study of starting powder by TGA under air with the same thermal cycle as the layer deposition. This decomposition scheme is shown in the following equation:



Although it is impossible to perform accurate TGA measurements directly on the layer, this method serves as a guide to estimate the values of δ for temperatures up to 1000°C . At 727°C , δ was found to be ~ 0.04 . Figure 3(a) shows that the heat treatment modified the value of δ slightly; however, the room-temperature value is close to 0.15, which is consistent with the value obtained using the Rice method. This result is in agreement with the value reported by Boehm *et al.*³⁸ for $\text{La}_2\text{NiO}_{4+\delta}$ powders. Furthermore, even if the evolution of δ under air suggests a possible reversible exchange of excess oxygen, more cycles of heating must be planned to conclude on oxygen reversibility.

(2) Texture of $\text{La}_2\text{NiO}_{4+\delta}$ Porous Layer

The analysis of ESEM images performed on a cross-sectional view shows that the real thickness of the layer is 5.4 μm . The

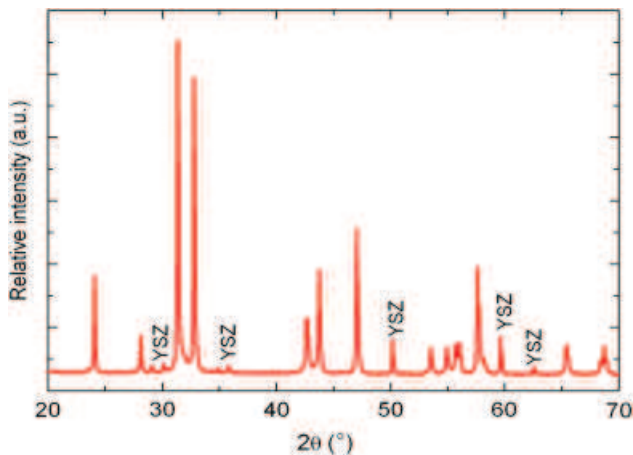


Fig. 2. X-ray diffraction pattern of the $\text{La}_2\text{NiO}_{4+\delta}$ layer at 300 K. The nonindexed peaks come from the $\text{La}_2\text{NiO}_{4+\delta}$ compound and the indexed peaks are the YSZ substrate.

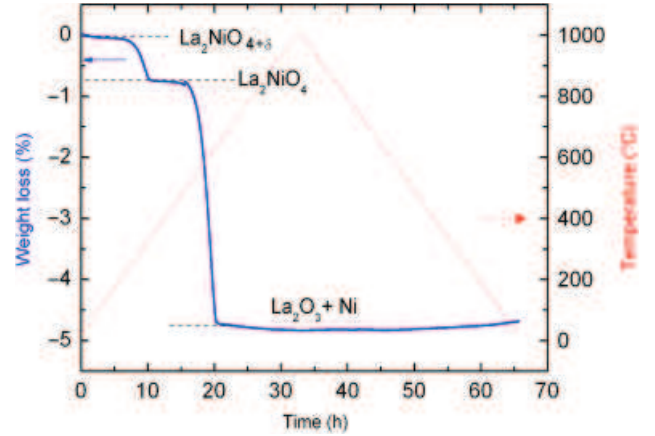


Fig. 3. Thermo-gravimetric analysis measurements under $\text{Ar}:\text{H}_2$ flow to determine the δ of the $\text{La}_2\text{NiO}_{4+\delta}$ starting powders.

top-view of this layer is presented in Fig. 5. This figure shows that the deposited layer is porous and that it is composed of single crystalline grains of around 500 nm in size that are homogeneously distributed on the surface. Thus, the relatively fine and uniform texture allows a regular distribution of the molecular oxygen over the entire volume of the $\text{La}_2\text{NiO}_{4+\delta}$ cathode.

The porosity of the layer was deduced from the ESEM image using the ImageJ[®] software. The porosity is found to be near 34% ($\pm 5\%$). However, this result can only be considered as a relative value because this method induces a misjudgment of the real total porosity of the coating and it cannot estimate the closed porosity of a layer. A ultra-small-angle X-ray scattering (USAXS) measurement could be performed to verify this result.

Figure 6 shows the 3D construction image of the surface layer by stereo imaging. Assuming that the roughness obeys a Gaussian distribution, and using the MEX software, we can extract from this image the statistical parameters¹⁰ that describe the surface roughness, e.g., the root-mean-square roughness ω_{rms} , the autocorrelation length τ and the Gaussian roughness surface slope α_{rms} . For this layer, ω_{rms} and τ were found to be 0.58 and 5.24 , respectively. Thus, α_{rms} of our layer was estimated to be 0.16 because $\alpha_{\text{rms}} = \sqrt{2 \frac{\omega_{\text{rms}}}{\tau}}$.

(3) Radiative Properties of $\text{La}_2\text{NiO}_{4+\delta}$ Porous Layer

Figure 7 shows the variation of normal spectral emissivity as a function of temperature for a 5.4 - μm -thick layer. The spectra were measured between 400 and 5000 cm^{-1} (i.e., 2 and 25 μm). This spectral domain corresponds to the range expected for a radiating body at temperatures from room temperature up to 900°C . Two domains can be easily distinguished. For wavenumbers lying between 400 and 2000 cm^{-1} , a broad band can be observed with an intensity that increases with increasing temperature. Then, for wavenumbers lying between 2000 and 5000 cm^{-1} , a plateau is observed with a level that increases upon heating. This plateau is typical of MIEC oxides having been observed previously in $\text{Pr}_2\text{NiO}_{4+\delta}$ thick porous layers (thickness ~ 30 μm).³⁹ When the temperature rises from 160 to 900°C , the normal total emissivity of the layer increases slightly from 0.76 to 0.79 (see the insert in Fig. 7). This value, which is rather high here, is calculated according to the following formula by assuming:

$$\varepsilon_{\sigma}^{\text{Total}}(T) = \frac{\int_{\sigma=0}^{\infty} \varepsilon_s(\sigma, T) L_s(\sigma, T) d\sigma}{\int_{\sigma=0}^{\infty} L(\sigma, T) d\sigma} \quad (4)$$

Such a value indicates that the intrinsic TRPs of the layer are sufficiently efficient to generate a broad absorption band in the mid-infrared range that corresponds to the second spectral domain and for the whole temperature range of this study. Note that, for the coating, the value of δ evolves from 0.15 at 20°C to 0.04 at 900°C . Thus, the value of δ should remain high enough

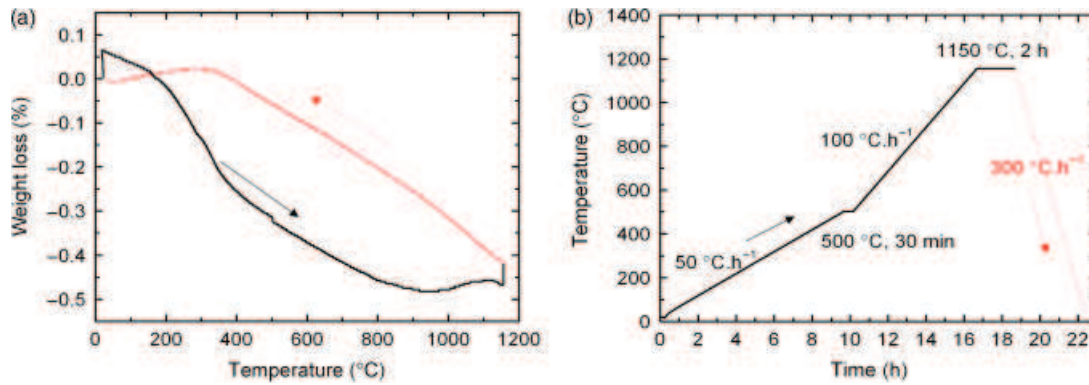


Fig. 4. Thermo-gravimetric analysis measurements in air in to simulate their evolution during (a) the deposition process and (b) a ramp heat treatment.

to preserve the optical activity of the polaronic carriers over the entire temperature range.

Figure 8 shows two spectra: the normal spectral emissivity of the analyzed samples (5.4 and 10.5 μm -thick layers) and that of the uncoated YSZ substrate at 727°C. The spectrum of the YSZ ceramic (thickness = 1 mm) is typical of a semitransparent oxide ceramic; its emissivity is high in the far-infrared due to phononic absorption (its emissivity is equal to unity at the Christiansen wavenumber) and then decreases exponentially in the mid-infrared range, to reach a very low emissivity at high wavenumbers. The addition of the $\text{La}_2\text{NiO}_{4+\delta}$ porous layer on the YSZ substrate modifies its original optical behavior over the spectral range covering the far- and the mid-infrared range. Note that according to a previous study,⁴⁰ the value of α_{rms} is equal to 0.16, which is less than the critical value of 0.28. Therefore, the surface roughness will not significantly influence the TRPs. Thus, we can conclude that surface roughness will not affect the modeling of the emissivity. The optical signature due to the

lattice vibration of the YSZ substrate can be viewed in the mid-infrared range (500–1500 cm^{-1}) of the spectrum corresponding to the semitransparent layer (5.4 μm thick—Fig. 8, red straight line). In contrast, this signature does not appear when the layer is opaque (10.5 μm thick—Fig. 8, blue dotted line). The spectrum is not deepened and behaves like a gray body. Between, these two spectra, the slight increase of the emissivity can be explained by the volumetric effect due to texture of the coating, as was shown in Rousseau *et al.*¹⁰

(4) Is the Layer Optically Thick?

To go one step further, it would be interesting to model the radiative behavior of this layer. However, one has to determine whether the infrared light emitted from the cathode is due to the layer itself or by a combination with the YSZ substrate. In other words, we should determine whether the layer is optically thick. The knowledge of the intrinsic TRPs of a single crystal of $\text{La}_2\text{NiO}_{4+\delta}$ provides an interesting guideline from which to start reasoning. We can begin by considering a grain of $\text{La}_2\text{NiO}_{4+\delta}$ and continue by looking at a collection of grains that produce a virtual layer of $\text{La}_2\text{NiO}_{4+\delta}$ with a similar texture to the real one described above (thickness, porosity etc ...).

In a previous work, the normal reflectivity spectra of a $\text{La}_2\text{NiO}_{4+\delta}$ single crystal as a function of temperature (20–723°C) in the *ab* plane and along the *c* axis were recorded and studied (see Ta *et al.*⁴⁰). It can be found that the $\text{La}_2\text{NiO}_{4+\delta}$ single crystal exhibits an anisotropic property. Thus, the electrically conductive behavior of the NiO_2 planes (said “*ab*” planes) and the rather insulating nature of the “*c*” axis influence the optical behavior of the single crystal. Thus, the *ab* planes have an important absorption coefficient over the whole spectral domain that is directly generated by the hole carriers, whereas the *c* axis has an absorption coefficient that is dominated by phononic mechanisms in the far-infrared range. For the *c* axis, the absorption mechanisms are rather low in the mid-infrared range, just as for any dielectric compound. Thus, a dense layer consisting of randomly oriented $\text{La}_2\text{NiO}_{4+\delta}$ grains (~ 500 nm) will have an absorption coefficient largely dominated by the optical contribution due to the *ab* plane. According to Mayerhöfer,⁴¹ the average complex dielectric function $\tilde{\epsilon}_{\text{poly}}(\sigma, T)$ will reflect the

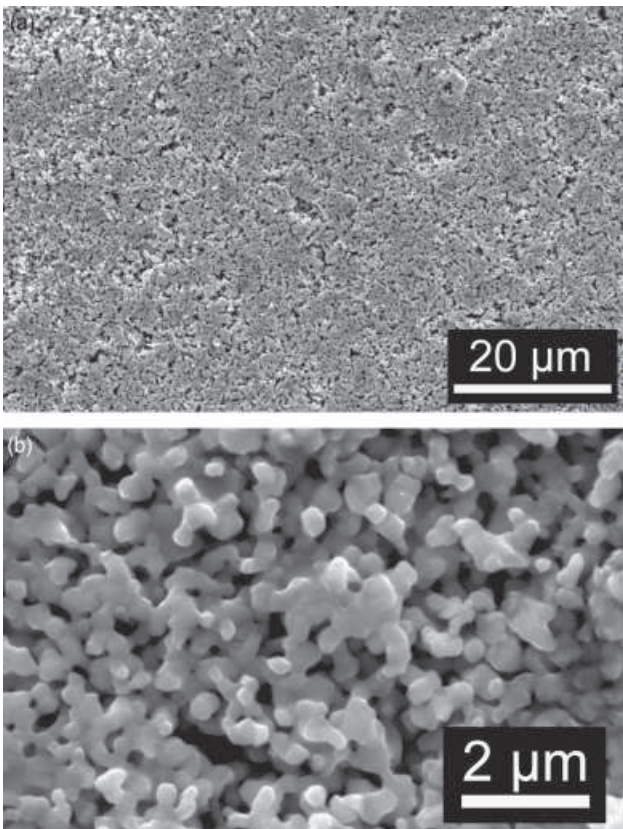


Fig. 5. Environmental scanning electron microscopy micrograph of the surface view for the $\text{La}_2\text{NiO}_{4+\delta}$ sample at 300 K with a magnification of $\times 1500$ (a) and of $\times 12000$ (b).

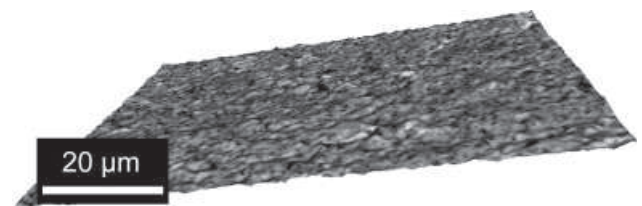


Fig. 6. Three-dimensional stereo imaging of a layer (5.4 μm thick) rebuilt by environmental scanning electron microscopy ($W \times H = 107 \mu\text{m} \times 69 \mu\text{m}$).

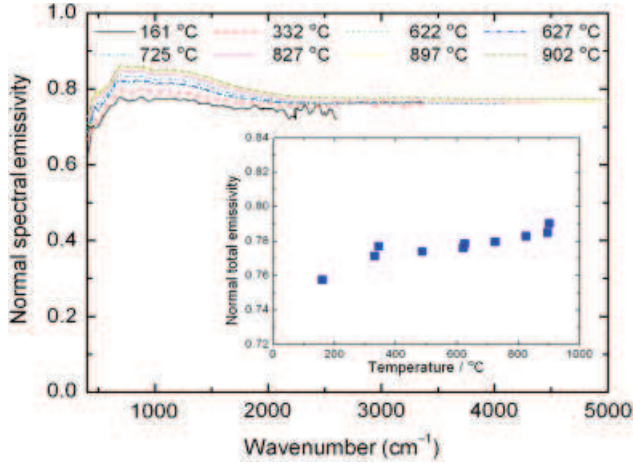


Fig. 7. Normal spectral emissivity at different temperatures for a 5.4- μm -thick layer. Insert: normal total emissivity as a function of temperature.

contributions from the ab planes and c axis. For ceramics with grains of about 500 nm, the absorption coefficient $K_{\text{poly}}(\sigma, T)$ is obtained by

$$K_{\text{poly}}(\sigma, T) = 4 \cdot \pi \cdot \sigma \cdot \Im(\sqrt{\tilde{\epsilon}_{\text{poly}}(\sigma, T)}) \\ = 4 \cdot \pi \cdot \sigma \cdot \Im\left(\sqrt{\frac{2}{3}\tilde{\epsilon}_{\text{ab}}(\sigma, T) + \frac{1}{3}\tilde{\epsilon}_{\text{c}}(\sigma, T)}\right) \quad (5)$$

where $\tilde{\epsilon}_{\text{poly}}(\sigma, T)$ is the mixed complex dielectric function of the ceramic, $\tilde{\epsilon}_{\text{ab}}(\sigma, T)$ is the complex dielectric due to the ab plane, and $\tilde{\epsilon}_{\text{c}}(\sigma, T)$ is the complex dielectric due to the c axis. \Im stands for the imaginary part of the complex dielectric function.

Next, let us consider the texture of the layer. As the size of grains and pores are < 500 nm, as revealed by ESEM, we can use the effective medium approximation for a range of wavelengths ranging between 2 and 20 μm (i.e., wavenumbers from 500 to 5000 cm^{-1}). For this purpose, the mixture law given by Bruggeman⁴² has been used:

$$(1-p) \frac{\tilde{\epsilon}_{\text{poly}}(\sigma, T) - \tilde{\epsilon}_{\text{eff}}(\sigma, T)}{\tilde{\epsilon}_{\text{poly}}(\sigma, T) + 2\tilde{\epsilon}_{\text{eff}}(\sigma, T)} \\ + p \frac{\tilde{\epsilon}_{\text{pore}}(\sigma, T) - \tilde{\epsilon}_{\text{eff}}(\sigma, T)}{\tilde{\epsilon}_{\text{pore}}(\sigma, T) + 2\tilde{\epsilon}_{\text{eff}}(\sigma, T)} = 0 \quad (6)$$

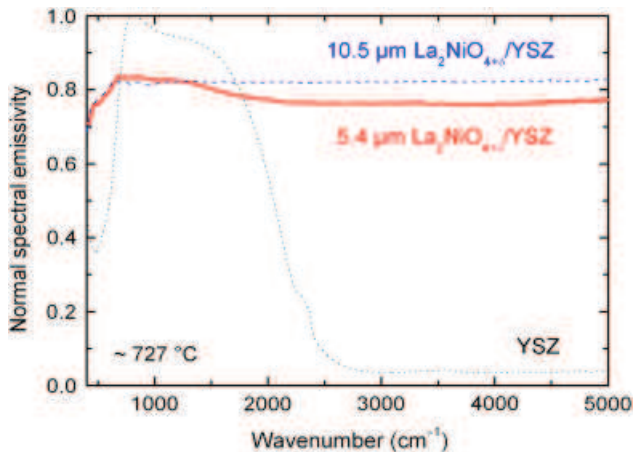


Fig. 8. Normal spectral emissivity at 727 $^{\circ}\text{C}$ obtained on an uncoated YSZ substrate and a $\text{La}_2\text{NiO}_{4+\delta}/\text{YSZ}$ sample.

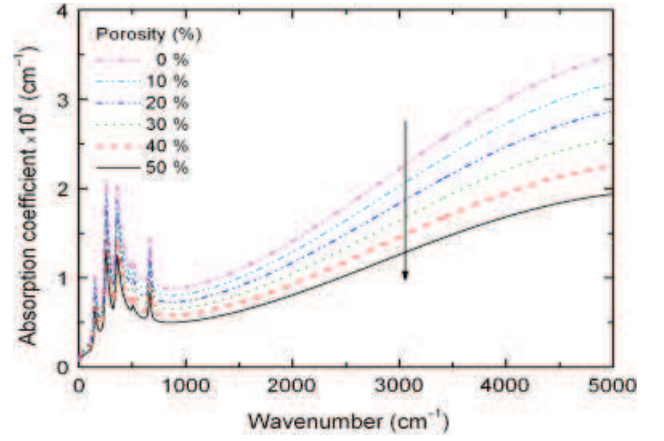


Fig. 9. Variation of absorption coefficient as a function of the porosity (modeling using $\delta = 0.11$).

where p is the porosity and $\tilde{\epsilon}_{\text{pore}}$ is equal to 1. In this equation, the pores are supposed to be spherical, which is a good approximation in view of the observations we made with ESEM (Fig. 5(b)). Similarly, we can define an effective absorption coefficient $K_{\text{eff}}(\sigma, T) = 4 \cdot \pi \cdot \sigma \cdot \text{Im}(\sqrt{\tilde{\epsilon}_{\text{eff}}})$

Figure 9 shows that the increase in porosity produces a decrease in the value of the absorption coefficient of a virtual ceramic of $\text{La}_2\text{NiO}_{4.11}$ at $T = 300$ K. The introduction of air (pores) in the ceramic increases the penetration depth of the infrared radiation. It should be noted that within the effective medium approximation, the phenomena related to light scattering are not taken into account. Supposing that the layer is opaque (transmittance $= e^{-K_{\text{eff}}d_{\text{layer}}} < 1\%$), a decrease of the absorption coefficient translates into an increase of the layer thickness. The minimum thickness for being optically thick was calculated to be ~ 9 μm for a sample of 34% porosity, which is consistent with the semitransparency seen for the 5.4 μm -thick layer. By assuming that the porosity of this kind of $\text{La}_2\text{NiO}_{4+\delta}$ layer is in the range 30%–40%, this cut-off value can be used as a criterion to distinguish a semitransparent radiative behavior from an opaque radiative behavior. Note that a great variety of $\text{La}_2\text{NiO}_{4+\delta}$ layers are produced today for electrochemical applications at high temperature (cathodic layers for SOFC, membrane for gaseous exchange) and their respective thicknesses can evolve between 0.6 μm ⁴³ and 200 μm .⁴⁴ Furthermore, for the specific case of SOFC, a current challenge is to reduce the thickness of the cathodic layer to few microns. What does this mean from a thermal point of view? If the cathodic layer is semitransparent, one has to know its optical thickness, its albedo, and its scattering phase function at the operating temperature of the cell in order to solve the radiation heat transfer issue.^{8,45–46} This task requires the use of the identification method,^{45,46} among others, to retrieve albedo and optical thickness from the knowledge of both the normal hemispherical reflectance and transmittance of the coating and by using the fact that light scattering is isotropic. In other words, more complex work is required in this case in order to carefully calculate the temperature field within the cell of a semitransparent layer in YSZ ceramic substrate—this substrate also exhibits optically thin behavior.⁸ In contrast, when the cathodic layer is sufficiently opaque—i.e., when the optical thickness is large enough ($> 4.6 = -\ln(1\%)$) as it has been defined previously, only knowledge of the emissivity is necessary to compute the radiative energy exchange, especially between the cell and the internal part of the metallic channel that transports reactive gas (oxygen for cathode). This calculation can be performed using the net radiosity method⁴⁶ assuming that each wall (the cathode and the internal channel) is opaque. However, as noted by Damm and Fedorov,⁵ “When one of the walls is a porous surface of the electrode, this assumption may be questionable

and the analysis becomes proportionally more complex.” This indicates that modeling the thermal field of the whole cell first requires a careful analysis of the material features (porosity, texture, chemical composition).

In the other hand, this study indicates that for the two layers of $\text{La}_2\text{NiO}_{4+\delta}$ (5.4 and 10.5 μm), even if the levels of their normal spectral emissivity appear as rather similar (see Fig. 8), their optical behavior is, in contrast, completely different. Ignoring this difference can lead to an incorrect interpretation of the heat transfer within the cell. Note that for $\text{La}_2\text{NiO}_{4+\delta}$ cathodes ($p \sim 30\%–40\%$) with a thickness $>9 \mu\text{m}$, their normal spectral emissivity must be very similar to the one of the 10.5 μm thick $\text{La}_2\text{NiO}_{4+\delta}$ layer. Furthermore, the modeling of the normal spectral emissivity of 5.4- μm thick $\text{La}_2\text{NiO}_{4+\delta}$ layer must take into account the YSZ substrate as well as the $\text{La}_2\text{NiO}_{4+\delta}$ layer.

Another important consideration to improve this work involves the method of measuring the porosity. Once the other key parameters, such as the thickness and δ , are fixed, the correct measurement of porosity is important. To this end, we are preparing to characterize the layer using USAXS at the Advanced Photon Source (Argonne, Argonne, IL).⁴⁷

Furthermore, we must also ensure that porosity remains stable within this temperature range. We must therefore verify whether or not the operating temperature of the cell can lead to an undesired sintering (decrease in porosity) for several cycles of heating. A similar study must also be scheduled for the oxygen excess (δ) for several cycles of use. The steadiness of these two parameters should lead to the thermal stability of the $\text{La}_2\text{NiO}_{4+\delta}$ layer.

V. Conclusions

An $\text{La}_2\text{NiO}_{4+\delta}$ porous layer was prepared by dip-coating with an appropriate ink including $\text{La}_2\text{NiO}_{4+\delta}$ powder. The textural parameters (porosity, surface roughness, and thickness) were investigated in addition to the chemical parameters (overstoichiometry, δ). The layer showed a thickness of 5.4 μm , porosity of 34% and oxygen over-stoichiometry of 0.14. The normal emittance spectra of the $\text{La}_2\text{NiO}_{4+\delta}$ layer at high temperatures (up to 900°C) were studied for the first time. The normal total emissivity of the layer increased from 0.76 to 0.79 with increasing temperature from 160 to 900°C. The influence of the textural parameters on the optical properties was also observed. The value obtained is typical of a gray body with a rather high emissivity. However, the porosity makes the layer semitransparent because it decreases the intrinsic value of the coefficient of absorption. Consequently, a computational modeling study on the radiative properties of this specific layer over the entire temperature range must be based on a bilayer model for dealing with both the optically thin YSZ substrate and optically thin $\text{La}_2\text{NiO}_{4+\delta}$ layer.

Acknowledgments

The authors would like to thank Mrs. A. Blin, M. P. Melin, and Mrs. S. Ory for their assistance, and Dr. M. Zaghrioui, Dr. M. Allix, and Dr. J. Drewitt for their helpful discussions. One of the authors acknowledges financial support from the “Région Centre” EOMAT (M. T. Ta), ANR project THERMASOFC JC07_190903 (J. Rolland), and the Basque Government for their support through the program of improvement of postdoctoral researchers of the Department of Education, Universities and Research (L. del Campo).

References

- ¹D. J. L. Brett, P. Aguiar, R. Clague, A. J. Marquis, S. Schöttl, R. Simpson, and N. P. Brandon, “Application of Infrared Thermal Imaging to the Study of Pellet Solid Oxide Fuel Cells,” *J. Power Sources*, **166** [1] 112–19 (2007).
- ²M. B. Pomfret, J. C. Owrutsky, and R. A. Walker, “In Situ Optical Studies of Solid-Oxide Fuel Cells,” *Annu. Rev. Anal. Chem.*, **3** [1] 151–74 (2010).
- ³R. Siegel and J. R. Howell, *Thermal Radiation Heat Transfer*. Taylor and Francis, Philadelphia, PA, 2001, 864pp.
- ⁴G. Brus and J. S. Szmyd, “Numerical Modelling of Radiative Heat Transfer in an Internal Indirect Reforming-Type SOFC,” *J. Power Sources*, **181** [1] 8–16 (2008).

- ⁵D. L. Damm and A. G. Fedorov, “Radiation Heat Transfer in SOFC Materials and Components,” *J. Power Sources*, **143** [1–2] 158–65 (2005).
- ⁶K. J. Daun, S. B. Beale, F. Liu, and G. J. Smallwood, “Radiation Heat Transfer in Planar SOFC Electrolytes,” *J. Power Sources*, **157** [1] 302–10 (2006).
- ⁷X. Lu, P. W. Faguy, and M. Liu, “In Situ Potential-Dependent FTIR Emission Spectroscopy,” *J. Electrochem. Soc.*, **149** [10] A1293–98 (2002).
- ⁸D. L. Damm and A. G. Fedorov, “Spectral Radiative Heat Transfer Analysis of the Planar SOFC,” *J. Fuel Cell Sci. Technol.*, **2** [4] 258–62 (2005).
- ⁹B. Rousseau, H. Gomart, D. De Sousa Meneses, P. Echegut, M. Rieu, R. Dugas, P. Lenormand, and F. Ansart, “Modelling of the Radiative Properties of an Opaque Porous Ceramic Layer,” *J. Electroceram.*, accepted (2010), doi: 10.1007/s10832-009-9595-6.
- ¹⁰B. Rousseau, H. Gomart, D. Zanghi, D. Bernard, and M. Stampanoni, “Synchrotron X-Ray μ -Tomography to Model the Thermal Radiative Properties of an Opaque Ceramic Coating at $T = 1000 \text{ K}$,” *J. Mater. Res.*, **25** [10] 1890–97 (2010).
- ¹¹L. Salvo, P. Cloetens, E. Maire, S. Zabler, J. J. Blandin, J. Y. Buffière, W. Ludwig, E. Boller, D. Bellet, and C. Jossier, “X-Ray Micro-Tomography an Attractive Characterisation Technique in Materials Science,” *Nucl. Instrum. Methods Phys. Res. B*, **200**, 273–86 (2003).
- ¹²M.-L. Fontaine, C. Laberty-Robert, F. Ansart, and P. Tailhades, “Elaboration and Characterization of $\text{La}_2\text{NiO}_{4+d}$ Powders and Thin Films via a Modified Sol-Gel Process,” *J. Solid State Chem.*, **177** [4–5] 1471–79 (2004).
- ¹³M. L. Fontaine, C. Laberty-Robert, M. Verelst, J. Pielaszeck, P. Lenormand, F. Ansart, and P. Tailhades, “Synthesis of $\text{La}_2\text{NiO}_{4+d}$ Oxides by Sol-Gel Process: Structural and Microstructural Evolution from Amorphous to Nanocrystallized Powders,” *Mater. Res. Bull.*, **41** [9] 1747–53 (2006).
- ¹⁴M. J. Escudero, A. Aguadero, J. A. Alonso, and L. Daza, “A Kinetic Study of Oxygen Reduction Reaction on $\text{La}_2\text{NiO}_{4+d}$ Cathodes by Means of Impedance Spectroscopy,” *J. Electroanal. Chem.*, **611** [1–2] 107–16 (2007).
- ¹⁵A. M. Hernández, L. Mogni, and A. Caneiro, “ $\text{La}_2\text{NiO}_{4+d}$ as Cathode for SOFC: Reactivity Study with YSZ and CGO Electrolytes,” *Int. J. Hydrog. Energy*, **35** [11] 6031–36 (2010).
- ¹⁶R. Sayers, R. A. De Souza, J. A. Kilner, and S. J. Skinner, “Low Temperature Diffusion and Oxygen Stoichiometry in Lanthanum Nickelate,” *Solid State Ion.*, **181** [8–10] 386–91 (2010).
- ¹⁷H. Zhao, F. Mauvy, C. Lalanne, J. M. Bassat, S. Fourcade, and J. C. Grenier, “New Cathode Materials for ITSOFC: Phase Stability, Oxygen Exchange and Cathode Properties of $\text{La}_{2-x}\text{NiO}_4$,” *Solid State Ion.*, **179** [35–36] 2000–5 (2008).
- ¹⁸D. E. Vladikova, Z. B. Stoyanov, A. Barbucci, M. Viviani, P. Carpanese, J. A. Kilner, S. J. Skinner, and R. Rudkin, “Impedance Studies of Cathode/Electrolyte Behaviour in SOFC,” *Electrochim. Acta*, **53** [25] 7491–99 (2008).
- ¹⁹E. Boehm, J. M. Bassat, M. C. Steil, P. Dordor, F. Mauvy, and J. C. Grenier, “Oxygen Transport Properties of $\text{La}_2\text{Ni}_{1-x}\text{Cu}_x\text{O}_{4+d}$ Mixed Conducting Oxides,” *Solid State Sci.*, **5** [7] 973–81 (2003).
- ²⁰A. Demourgues, P. Dordor, J. P. Doumerc, J. C. Grenier, E. Marquestaut, M. Pouchard, A. Villesuzanne, and A. Wattiaux, “Transport and Magnetic Properties of $\text{La}_2\text{NiO}_{4+d}$ ($0 < d \leq 0.25$),” *J. Solid State Chem.*, **124** [2] 199–204 (1996).
- ²¹N. Poirot-Reveau, P. Odier, P. Simon, and F. Gervais, “Signature of Stripes in the Optical Conductivity of $\text{La}_2\text{NiO}_{4.11}$,” *Phys. Rev. B*, **65**, 094503, 9pp (2002).
- ²²D. E. Rice and D. J. Buttrey, “An X-Ray Diffraction Study of the Oxygen Content Phase Diagram of $\text{La}_2\text{NiO}_{4+d}$,” *J. Solid State Chem.*, **105** [1] 197–210 (1993).
- ²³J. M. Bassat, P. Odier, A. Villesuzanne, C. Marin, and M. Pouchard, “Anisotropic Ionic Transport Properties in $\text{La}_2\text{NiO}_{4+d}$ Single Crystals,” *Solid State Ion.*, **167** [3–4] 341–47 (2004).
- ²⁴C. C. Homes, J. M. Tranquada, and D. J. Buttrey, “Stripe order and Vibrational Properties of $\text{La}_2\text{NiO}_{4+d}$ for $d = 2/15$: Measurements and Ab Initio Calculations,” *Phys. Rev. B*, **75** [4] 045128, 11pp (2007).
- ²⁵J. D. Jorgensen, B. Dabrowski, S. Pei, D. R. Richards, and D. G. Hinks, “Structure of the Interstitial Oxygen Defect in $\text{La}_2\text{NiO}_{4+d}$,” *Phys. Rev. B*, **40**, 2187–99 (1989).
- ²⁶B. Rousseau, M. Chabin, P. Echegut, A. Sin, F. Weiss, and P. Odier, “High Emissivity of a Rough Pr_2NiO_4 Coating,” *Appl. Phys. Lett.*, **79**, 3633–6 (2001).
- ²⁷D. A. Crandles, T. Timusk, J. D. Garret, and J. E. Greedan, “Temperature Dependence of the Mid-Infrared Absorption in $\text{La}_{1.84}\text{Sr}_{0.16}\text{NiO}_{4+d}$,” *Phys. C*, **216** [1–2] 94–8 (1993).
- ²⁸H. Tamura, A. Hayashi, and Y. Ueda, “Phase Diagram of $\text{La}_2\text{NiO}_{4+d}$ ($0 < d < 0.18$): I. Phase at Room Temperature and Phases Transition Above $d = 0.15$,” *Phys. C*, **216** [1–2] 83–8 (1993).
- ²⁹X.-X. Bi, P. C. Eklund, and J. M. Honig, “Doping Dependence of the A-B Plane Optical Conductivity of Single-Crystal $\text{La}_{2-x}\text{Sr}_x\text{NiO}_{4+d}$,” *Phys. Rev. B*, **48**, 3470–8 (1993).
- ³⁰B. Rousseau, D. De Sousa Meneses, A. Blin, M. Chabin, P. Echegut, P. Odier, and F. Gervais, “High-Temperature Behavior of Infrared Conductivity of a $\text{Pr}_2\text{NiO}_{4+d}$ Delta Single Crystal,” *Phys. Rev. B*, **72**, 104114, 6pp (2005).
- ³¹S. Castillo, R. F. Cienfuegos, M. L. Fontaine, P. Lenormand, P. Bacchin, and F. Ansart, “Influence of the Processing Parameters of Slurries for the Deposit of Nickelate Thick Films,” *Mater. Res. Bull.*, **42** [12] 2125–31 (2007).
- ³²M. L. Fontaine, C. Laberty-Robert, F. Ansart, and P. Tailhades, “Composition and Porosity Graded $\text{La}_{2-x}\text{NiO}_{4+d}$ ($x \geq 0$) Interlayers for SOFC: Control of the Microstructure via a Sol-Gel Process,” *J. Power Sources*, **156** [1] 33–8 (2006).
- ³³O. Rozenbaum, D. De Sousa Meneses, Y. Auger, S. Chermanne, and P. Echegut, “A Spectroscopic method to Measure the Spectral Emissivity of Semi-Transparent Materials up to High Temperature,” *Rev. Sci. Instrum.*, **70** [10] 4020–25 (1999).
- ³⁴D. De Sousa Meneses, J.-F. Brun, B. Rousseau, and P. Echegut, “Polar Lattice Dynamics of the MgAl_2O_4 Spinel up to the Liquid State,” *J. Phys.: Condens. Matter.*, **18** [24] 5669–86 (2006).

- ³⁵L. del Campo, D. De Sousa Meneses, A. Blin, B. Rousseau, E. Véron, M. Balat-Pichelin, and P. Echegut, "High Temperature Radiative Properties of an Yttria-Stabilized Hafnia Ceramic," *J. Am. Ceram. Soc.*, (2011) (in press).
- ³⁶A. Aguadero, J. A. Alonso, M. T. Fernández-Díaz, M. J. Escudero, and L. Daza, "In Situ High Temperature Neutron Powder Diffraction Study of $\text{La}_2\text{Ni}_{0.6}\text{Cu}_{0.4}\text{O}_{4+d}$ in Air: Correlation with the Electrical Behaviour," *J. Power Sources*, **169** [1] 17–24 (2007).
- ³⁷M. Hücker, K. Chung, M. Chand, T. Vogt, J. M. Tranquada, and D. J. Buttrey, "Oxygen and Strontium Codoping of La_2NiO_4 : Room-Temperature Phase Diagrams," *Phys. Rev. B.*, **70**, 064105, 10pp (2004).
- ³⁸E. Boehm, J.-M. Bassat, P. Dordor, F. Mauvy, J.-C. Grenier, and P. Stevens, "Oxygen Diffusion and Transport Properties in Non-Stoichiometric $\text{Ln}_{2-x}\text{NiO}_{4+\delta}$ Oxides," *Solid State Ion.*, **176** [37–38] 2717–25 (2005).
- ³⁹B. Rousseau, J. Brun, D. Meneses, and P. Echegut, "Temperature Measurement: Christiansen Wavelength and Blackbody Reference," *Int. J. Thermophys.*, **26** [4] 1277–86 (2005).
- ⁴⁰M. T. Ta, J. Y. Rolland, P. Echegut, B. Rousseau, M. Zaghrioui, F. Giovannelli, H. Gomart, P. Lenormand, and F. Ansart, "Optical Properties of $\text{La}_2\text{NiO}_{4+\delta}$ Single Crystal on Temperature (300–1000 K) and Modeling to Predict the Radiative Properties," *Appl. Phys. Lett.*, **97** [18] 181917, 3pp (2010).
- ⁴¹T. G. Mayerhöfer, "New Method of Modeling Infrared Spectra of Non-Cubic Single-Phase Polycrystalline Materials with Random Orientation," *Appl. Spectrosc.*, **56**, 1194–205 (2002).
- ⁴²D. A. G. Bruggeman, "The Calculation of Various Physical Constants of Heterogeneous Substances I. The Dielectric Constants and Conductivities of Mixtures Composed of Isotropic Substances," *Ann. Phys.*, **416** [7] 636–64 (1935).
- ⁴³V. Faucheux, M. Audier, and S. Pignard, "Physical Properties of Epitaxial $\text{La}_2\text{NiO}_{4+d}$ Thin Films," *Appl. Surf. Sci.*, **252** [15] 5504–7 (2006).
- ⁴⁴A. L. Shaula, E. N. Naumovich, A. P. Viskup, V. Pankov, A. V. Kovalevsky, and V. V. Kharton, "Oxygen Transport in $\text{La}_2\text{NiO}_{4+\delta}$: Assessment of Surface Limitations and Multilayer Membrane Architectures," *Solid State Ion.*, **180** [11–13] 812–16 (2009).
- ⁴⁵L. A. Dombrovsky and D. Baillis, *Thermal Radiation in Disperse Systems: An Engineering Approach*. Begellhouse, Redding, CT, 2010, 689pp.
- ⁴⁶M. F. Modest, *Radiative Heat Transfer (Second Edition)*. Academic press (Elsevier Science), San Diego, CA, 2003, 822pp.
- ⁴⁷J. Ilavsky, "Characterization of Complex Thermal Barrier Deposits Pore Microstructures by a Combination of Imaging, Scattering, and Intrusion Techniques," *J. Therm. Spray Technol.*, **19** [1] 178–89 (2010). □